ELSEVIER

22 July 1996

PHYSICS LETTERS A

Physics Letters A 217 (1996) 305–314

An experimental demonstration of resonant sideband extraction for laser-interferometric gravitational wave detectors

G. Heinzel [1], J. Mizuno [2], R. Schilling, W. Winkler, A. Rüdiger, K. Danzmann [3]

Max-Planck-Institut für Quantenoptik, Hans-Kopfermann-Strasse 1, D-85748 Garching, Germany

Received 29 February 1996; accepted for publication 30 April 1996
Communicated by P.R. Holland

Abstract

Resonant sideband extraction is a new optical configuration for laser-interferometric gravitational wave detectors with Fabry–Perot cavities in the arms. It reduces the thermal load on the beam splitter and the coupling mirrors of the cavities and also allows one to adapt the frequency response of the detector to a variety of requirements. We report the first experimental demonstration using a table-top setup at a *detuned* operating point. An increase of sensitivity by 6 dB was observed for artificial signals at frequencies above the arm cavity bandwidth, and the overall transfer function agreed well with theoretical predictions.

PACS: 04.80.Nn; 07.60.Ly; 42.25.Hz; 95.55.Ym
Keywords: Resonant sideband extraction; Michelson interferometer; Fabry–Perot; Mach–Zehnder; Gravitational wave detector; Three-mirror cavity

1. Introduction

Direct detection of gravitational waves by laser interferometry seems possible within the next several years. Construction work has begun for several large detectors (e.g. LIGO in the U.S. [1], VIRGO [2] and GEO600 [3] in Europe, and others). One fundamental limit for the sensitivity of any optical detector is given by the photon counting error (*shot noise*). In order to achieve the desired high sensitivity, various extensions to the basic Michelson interferometer have been proposed, such as delay lines or Fabry–Perot cavities in the arms, power- and signal-recycling [4,5]. It can be shown [6] that for any of these configurations the shot-noise limited sensitivity (expressed as linear spectral density $\tilde{h}$ of strain in space producing the same output signal as the intrinsic detector noise) is proportional to $\sqrt{\Delta f_{\mathrm{BW}}/E}$, where E is the amount of light

[1] E-mail: ghh@mpq.mpg.de.
[2] E-mail: mizuno@mpq.mpg.de.
[3] Also at Universität Hannover, Institut für Atom- und Molekülphysik, Appelstrasse 2, D-30167 Hannover, Germany.

PII S0375-9601(96)00361-1

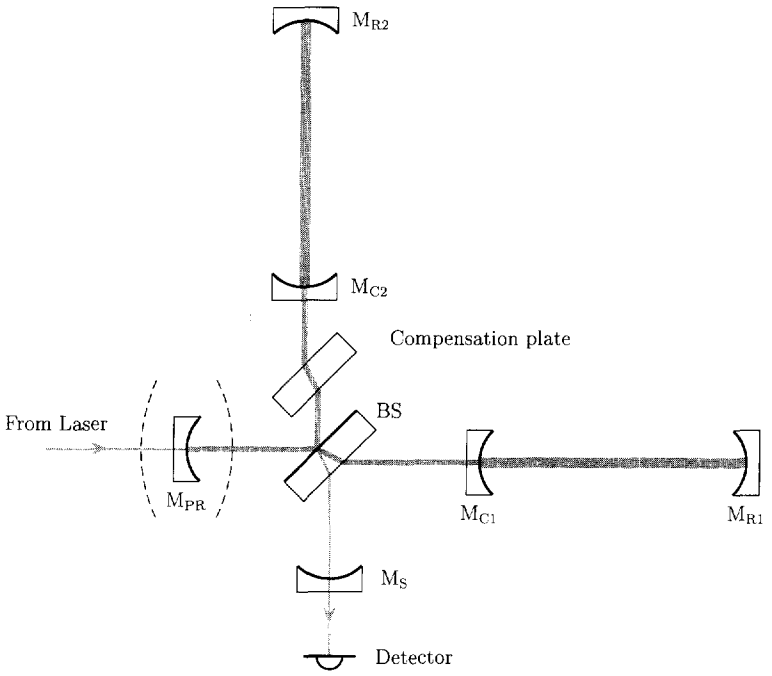

Fig. 1. Optical layout for resonant sideband extraction. Power recycling (with mirror M_{PR}) is an option not affecting the principle of RSE. The compensation plate may be included for reasons of symmetry between the two arms.

energy stored in the arms, and Δf_{BW} the detector bandwidth. All of the above mentioned schemes amount to increasing E for a given physical arm length and laser power and/or modifying the detector bandwidth.

Among these schemes, power recycling is considered indispensable for all of the planned large detectors. The power gain achievable will, however, be limited by imperfect contrast as well as losses in the substrates of the beam splitter (and those of the arm cavity coupling mirrors). Furthermore, the high-power beam may cause absorption-induced thermal lensing and birefringence in the substrates [7–9].

By using high-finesse Fabry–Perot arm cavities, the high-power beam is confined to within the arm cavities and is not transmitted through any substrate. The usable finesse of the arm cavities was, however, believed to be limited by the required detector bandwidth.

Resonant sideband extraction (RSE) [6,10] was proposed as a new optical configuration to overcome this limitation. In particular, the detector bandwidth can be made broader than the arm-cavity bandwidth, thereby permitting the use of high-finesse cavities in the arms. There exist non-detuned and detuned modes of operation, where "tuned" in this paper refers to making the signal extraction cavity resonant for the carrier, which yields the broadest possible detector bandwidth. The "detuned" modes permit a sensitivity peak to be obtained at an adjustable frequency.

The outline of this paper is as follows: In Section 2, we describe the frequency response of RSE, closely following Ref. [6]. Our experimental setup is described in Section 3. The results are discussed in Section 4.

2. Frequency response of resonant sideband extraction

Fig. 1 shows the basic optical layout for RSE. It resembles that of signal recycling with Fabry–Perot cavities in the arms, but here a different sub-wavelength positioning of the signal extraction mirror (M_S in Fig. 1)

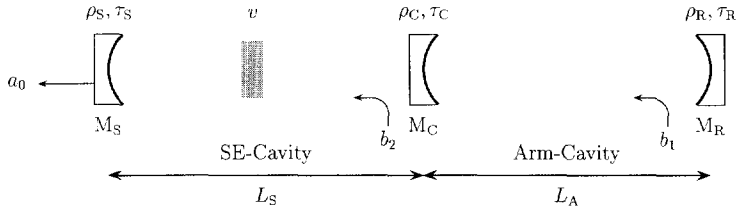

Fig. 2. Three-mirror cavity storing the signal sidebands.

produces a different effect, as described below.

To simplify the analysis, we assume all interfering beams to have the same polarization and transverse mode structure. To compute the frequency response, we also assume a 50/50 beam splitter, both arm cavities to be identical and in resonance with the incoming light of angular frequency ω_0 (the "carrier"). Furthermore, we assume the interferometer to be operated at a dark fringe (at the detector port), i.e. all carrier light returning from the arms is interfering constructively towards the laser (or power-recycling mirror). Note that the amplitude reflectivity of the Michelson interferometer as a whole seen from either port is identical (if the beam splitter's transmittance equals its reflectivity), whatever the arms are.

A suitably oriented and polarized gravitational wave produces a phase modulation of opposite sign in the two arms. In the following we consider only a single frequency component of angular frequency ω_g. The phase modulation sidebands at $\omega_0 \pm \omega_g$ interfere constructively towards the signal extraction mirror M_S. After being reflected by M_S, they re-enter the interferometer, which in turn reflects them back to M_S. The signal sidebands are thus stored in a "split" cavity [11] composed of the Michelson interferometer and M_S. Under the above assumptions, this split cavity is equivalent to a *three-mirror cavity* (Fig. 2) formed by M_S, M_C and M_R, where the two identical arm cavities have been "folded" together to form a single cavity consisting of M_C and M_R. (The notations in Fig. 2 are explained in the context of Eqs. (1) and (2)).

One possible interpretation of this three-mirror cavity is to consider the cavity as being composed of M_R and a *compound mirror* formed by M_S and M_C. The compound mirror (which we also call the "signal extraction cavity") has frequency-dependent transmittance and reflectivity. In *signal recycling*, this cavity is tuned to "anti-resonance" (i.e. centered between two successive resonances) so as to obtain a *lower* transmittance than that of M_C alone, resulting in an *increased* storage time for the signal.

The purpose of RSE, on the other hand, is to *reduce* the storage time for the signal, in order to allow long storage times for the carrier without sacrificing detector bandwidth. This can be achieved by tuning the signal extraction cavity to resonance so that its transmittance for the signal frequencies of interest is *higher* than that of M_C alone. For these frequencies the storage time in the three-mirror cavity is shorter than that in the unmodified arm cavity. In the non-detuned case, this reduction of the storage time results in an increased bandwidth.

To compute the frequency response we consider the light amplitudes going to and from each mirror in the scalar model (see Fig. 2). As input to the cavity we have b_1, which represents the signal sidebands produced by differential phase modulation of the carrier (e.g. by gravitational waves) in the arms. Of importance in our experiment is also a further input b_2, which corresponds to phase modulation sidebands produced between the beam splitter and arm cavity. Note that the carrier (in an ideal dark-fringe operation) never reaches M_S and therefore is not considered in this picture.

The amplitudes at the different points are coupled by a set of linear equations. Solving this set for the output amplitude a_0 yields the transfer functions

$$G_1(\omega,\delta) = \frac{a_0}{b_1} = \frac{\tau_C\tau_S v e^{i\omega(T_A+T_S)}}{1-\rho_R\rho_C e^{2i\omega T_A} - \rho_C\rho_S v^2 e^{i(2\omega T_S+\delta)} + \rho_R\rho_S v^2 e^{i[2\omega(T_A+T_S)+\delta]}}, \tag{1}$$

for signals fed into the arm cavity (setting $b_2 = 0$), and

$$G_2(\omega,\delta)=\frac{a_0}{b_2}=\frac{\tau_S v e^{i\omega T_S}(1-\rho_R\rho_C e^{2i\omega T_A})}{1-\rho_R\rho_C e^{2i\omega T_A}-\rho_C\rho_S v^2 e^{i(2\omega T_S+\delta)}+\rho_R\rho_S v^2 e^{i[2\omega(T_A+T_S)+\delta]}}, \tag{2}$$

for signals fed into the signal extraction cavity (setting $b_1 = 0$). Here τ and ρ denote the amplitude transmission and reflection coefficients of the respective mirrors. The angular frequency ω denotes the light frequency offset with respect to the carrier frequency (thus $\omega = \pm\omega_g$ for the upper and lower sideband, respectively). The phase δ represents the detuning of the signal extraction cavity, with $\delta = 0$ for non-detuned (broadband) RSE, $\delta = \pi$ for signal recycling and all other values representing detuned cases. $T_S = L_S/c$ and $T_A = L_A/c$ are the one-way light travel times in the signal extraction cavity and arm cavity, respectively. The losses of the arm cavity are modeled by a finite transmittance of the rear mirror $0 < \tau_R^2 \ll 1$, and the losses in the signal extraction cavity (beam splitter, imperfect contrast, etc.) by an amplitude transmittance $v \lessapprox 1$. If the signal is a true gravitational wave acting on the whole length of the cavity, G_1 must be multiplied by the factor $\sin(\omega T_A)/\omega T_A$ (see e.g. Ref. [12]), which can however be neglected for our experiment.

We use external modulation (see e.g. Ref. [13] and references therein) to detect the signal sidebands in our experiment. In the Mach–Zehnder interferometer used for this purpose, the light eventually leaving the Michelson interferometer through M_S, with amplitude a_s, is superimposed with a reference beam that has been phase modulated at an angular frequency ω_e. A relative phase shift ψ is introduced between signal and reference beam before they are superimposed in order to adjust for maximum output signal. Synchronous demodulation of the resulting photocurrent at the modulation frequency ω_e produces an output signal given by

$$y = y_0[\mathrm{Re}(a_s)\sin\psi + \mathrm{Im}(a_s)\cos\psi] = y_0\,\mathrm{Im}(a_s e^{i\psi}), \tag{3}$$

where all constant factors have been included in y_0.

The signal wave a_s consists of two sidebands a_+ and a_-, which are not necessarily symmetric in the detuned cases of RSE (or signal recycling),

$$a_s = i a_+ e^{i\omega_g t} + i a_- e^{-i\omega_g t}. \tag{4}$$

The factors i arise from setting the carrier phase to zero. For the output signal as detected by external modulation we get from Eqs. (3) and (4),

$$y = \mathrm{Re}(A e^{i\omega_g t}), \qquad \text{with } A = a_+ e^{i\psi} + a_-^* e^{-i\psi}, \tag{5}$$

where A represents the complex amplitude of the *output signal* of frequency ω_g [6]. The asterisk denotes complex conjugation.

Thus the transfer function of the interferometer up to the demodulated detector output for phase modulation signals of frequency ω_g generated inside either the arm cavity or signal extraction cavity is given (neglecting common constant factors) by

$$H_1(\omega_g,\delta,\psi) = G_1(\omega_g,\delta)\,e^{i\psi} + G_1^*(-\omega_g,\delta)\,e^{-i\psi}, \tag{6}$$

$$H_2(\omega_g,\delta,\psi) = G_2(\omega_g,\delta)\,e^{i\psi} + G_2^*(-\omega_g,\delta)\,e^{-i\psi}, \tag{7}$$

since both sidebands have been produced with the same amplitude by the phase modulation.

Note that the transfer function of the interferometer depends on ψ, the relative phase between signal wave and reference wave. This becomes important in detuned cases of RSE (or signal recycling), where both sidebands will generally have different amplitudes. One extreme is the "single sideband" case, where the signal wave a_s is dominated by only one of the two sidebands. This approximately happens near the sensitivity peak of a detuned interferometer. Then the dependence on ψ is small, as can be seen from Eq. (5) by setting $a_- = 0$.

When the two sidebands have comparable amplitudes, however, the amount of detected output signal depends sinusoidally on ψ. It turns out that there is not one fixed optimum detection phase ψ for all signal frequencies

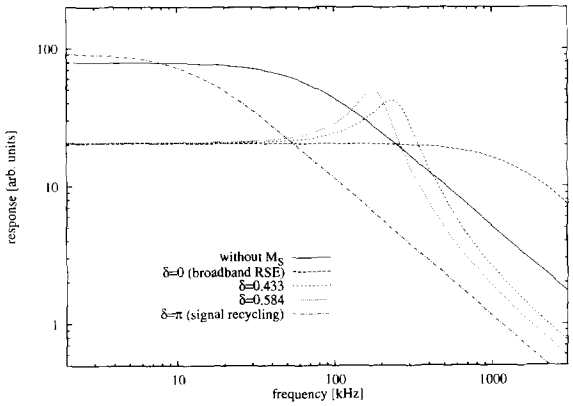

Fig. 3. Calculated frequency response of our table-top interferometer.

simultaneously. The difference between the optimum ψ for low and for high frequencies (in relation to the peak frequency) is roughly $\pi/2$.

Fig. 3 shows the computed frequency response $|H_1(\omega, \delta, \psi = 0)|$ of our table-top interferometer, using the parameters given in the next section. We have plotted the responses for the non-detuned cases of RSE and signal recycling ($\delta = 0$ and $\delta = \pi$, respectively), two detuned operating points used in our experiment, and the response without any mirror M_S for comparison. For a clear experimental demonstration of an *increase* in sensitivity we chose the detuned operating points, since test signals were applied by a PZT having a few 100 kHz bandwidth at most. Furthermore, the characteristic peaks in the frequency response allow a better comparison with theory. In order to eliminate the effect of PZT resonances we compared the response with M_S locked to its proper position to the response with M_S removed.

3. Experiment

In our experiment (Fig. 4), the interferometer was illuminated by approximately 300 mW of single-mode light at 514.5 nm from an INNOVA-90 Ar^+ Laser through two Faraday isolators (made by Optics for Research). Its frequency can be controlled by an intra-cavity Pockels cell and a slow PZT shifting one mirror. The light is phase modulated at 12 MHz by a Gsänger PM-25 Pockels cell PC1, with a modulation index of approximately 0.25 rad. The arm cavities (length 40 cm) consist of flat coupling mirrors (M_{C1} and M_{C2}) with 1850 ppm power transmittance (measured average), and curved reflectors (M_{R1} and M_{R2}, $R = 1$ m) mounted on massive aluminum cylinders. Total cavity losses (excluding τ_C^2) were measured as 350 ppm (the main loss originating from the coating of the rear reflecting mirrors), yielding a finesse of approximately 3000 and a power reflectivity of the cavities of about 50% at resonance. With two mode-matching lenses, more than 90% of the incoming power was coupled into the cavity's fundamental mode.

Glass plates (BP1 and BP2) mounted almost under the Brewster angle reflect 0.5% of the light power returning from the cavities to the photodetectors PD1 and PD2. Their photocurrents are demodulated at 12 MHz and used for stabilization of the laser frequency and the second cavity's length, employing the Pound–Drever method [14]. The system was operated in air and thus very sensitive to acoustic disturbances, necessitating high gain and broad bandwidth for those loops. The first loop (with PD1) locks the laser to the first cavity with a unity-gain frequency of approximately 120 kHz. The second loop (with PD2) locks the length of the second cavity to the laser by adjusting the cavity's length with one slow high-efficiency and one fast PZT, the latter being mounted on an acoustic delay line to reduce low-frequency mechanical resonances. This loop had a unity gain frequency of approximately 40 kHz.

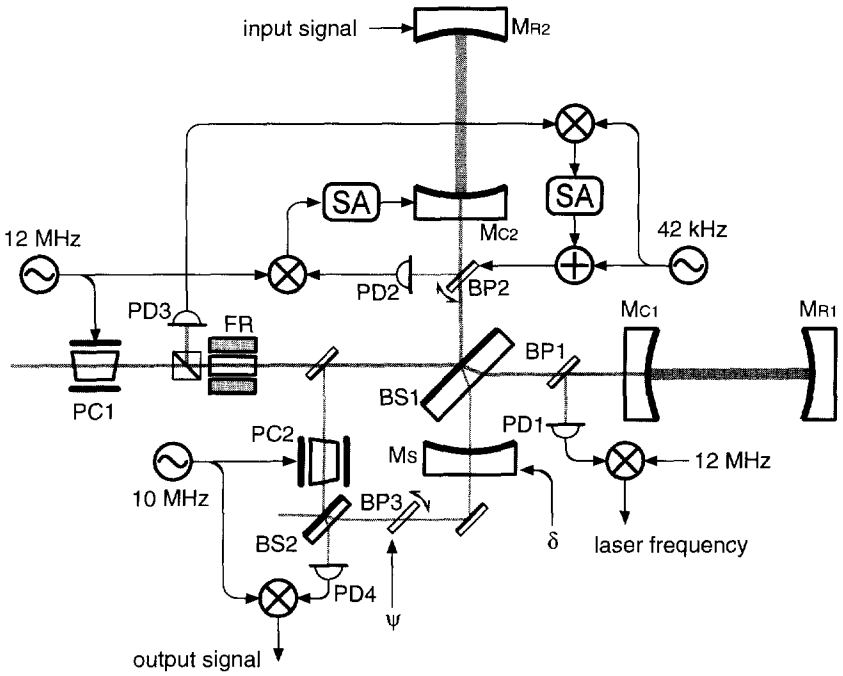

Fig. 4. Simplified diagram of our experimental setup, showing only the control loops for the arm cavities and the Michelson interferometer. FR is a Faraday rotator, PC are Pockels cells, ⊖, ⊕ and ⊗ electronic oscillators, adders and mixers respectively, BS are beam splitters, BP are glass plates in or near the Brewster angle, PD photodiodes and SA servo amplifiers. See also Fig. 5.

A phase modulation of 42 kHz (*internal modulation*) was applied between the beam splitter and the second cavity by dithering the Brewster plate BP2, which was mounted on a galvanometer scanner allowing tilting about small angles. A tilt of 0.03° was sufficient to change the optical path length by $\lambda/2$, and the modulation index at 42 kHz was approximately 5 mrad. The light returning towards the laser was directed onto photodetector PD3 by one of the Faraday isolators. The photocurrent was demodulated at 42 kHz and fed back to BP2 through an appropriate filter in order to lock the Michelson interferometer to a dark fringe at its output. The unity-gain frequency of this loop was approximately 700 Hz. Another purpose of this 42 kHz modulation is to continually adjust the external modulation's phase relationship, as described below. With both arm cavities locked, the interference minimum was approximately 1% of the power at the maximum.

Test signals up to 500 kHz were fed into the interferometer at the fast PZT holding M_{R2}. This phase modulation in only one arm can be separated into two components of equal magnitude, a common mode component directed towards the laser, and a differential component, which represents the signal of interest. The reference beam for the external modulation was taken from the light returning towards the laser and was phase modulated at 10 MHz ($= \omega_e/2\pi$) by another PM-25 Pockels cell (PC2 in Fig. 4). The relative phase ψ between signal and reference beam was introduced via another galvanometer-tilted Brewster plate BP3. After synchronous demodulation (at 10 MHz), the photocurrent of photodetector PD4 represents the interferometer's output signal.

The phase ψ was controlled so as to maximize the amplitude of the 42 kHz component in the output signal originating from the phase modulation at BP2. The amplitude at 42 kHz was detected by synchronous demodulation of the interferometer output at 42 kHz. This amplitude was maximized by dithering ψ with 260 Hz, demodulating the 42 kHz amplitude at 260 Hz and feeding back the resulting error signal to BP3 through an appropriate loop filter. This loop is not shown in Figs. 4 and 5.

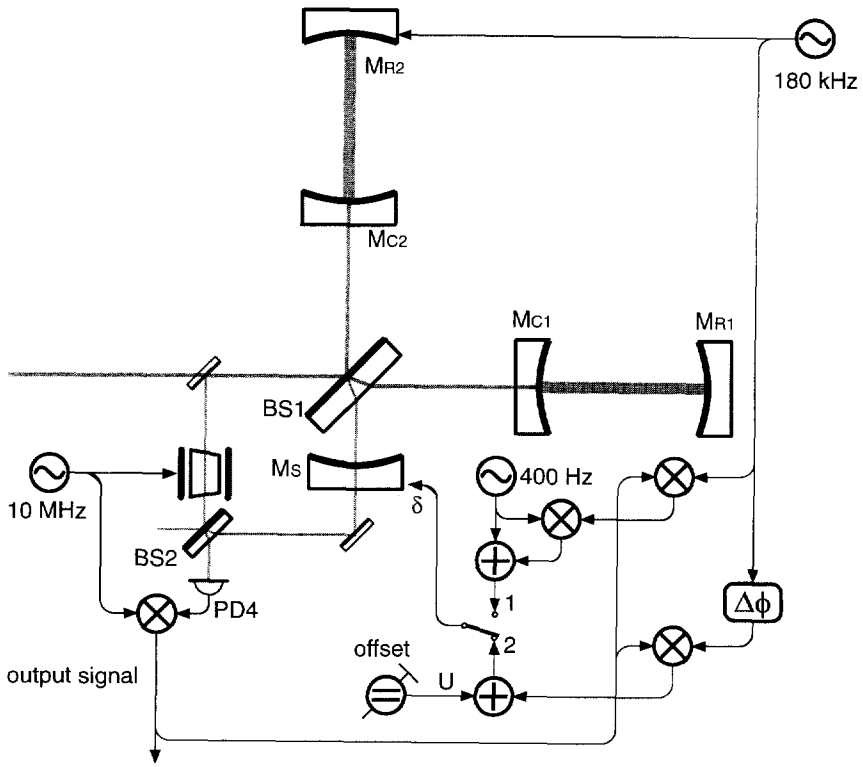

Fig. 5. Control loops for the signal extraction mirror M_S. In addition to the symbols used in Fig. 4, $\Delta\phi$ represents an electronic phase shifter and $\ominus$ an adjustable DC voltage.

The curved signal extraction mirror M_S ($R = 1$ m) had a power reflectivity of 82% and was placed 40 cm away from the flat mirrors M_{C1} and M_{C2}, so that its curvature matched the wavefront curvature. The amplitude loss factor of the signal extraction cavity, v in Eqs. (1) and (2), was estimated as $\sqrt{1-0.005}$, taking only the losses by BP1 and BP2 into account. The influence of this factor on the frequency response is small.

Two different schemes to lock the position of M_S (using another PZT) were investigated. Both schemes use a 180 kHz calibration signal (with an amplitude corresponding to less than 1 pm movement), which was also fed to M_{R2} (see Fig. 5).

The first scheme (switch position 1 in Fig. 5) was aiming at a peak sensitivity at 180 kHz. The amplitude of the 180 kHz calibration signal at the output was detected by synchronous demodulation. In a scheme similar to the control of ψ described above, the position of M_S was dithered with 400 Hz. The 180 kHz amplitude was again synchronously demodulated at 400 Hz to obtain an error signal, which was fed back to M_S. For real gravitational wave detectors, this scheme will not be the best choice, since one presumably will not want to introduce test signals just at the sensitivity peak, and because the frequency of that peak needs to be dithered to obtain an error signal.

The scheme was, however, useful to acquire lock of the different coupled loops and to adjust the electronics for the second scheme (switch position 2 in Fig. 5). Here M_S is no longer dithered, but instead controlled in such a way as to maintain the amplitude of the 180 kHz signal at the output at a predefined constant level U, similar to a concept initially proposed by Strain for the use with signal recycling [15]. The 180 kHz amplitude is again obtained by synchronous demodulation, now, however, with a different and adjustable demodulation phase $\Delta\phi$. If the level U is chosen somewhere between the extreme amplitude values, the error signal obtained

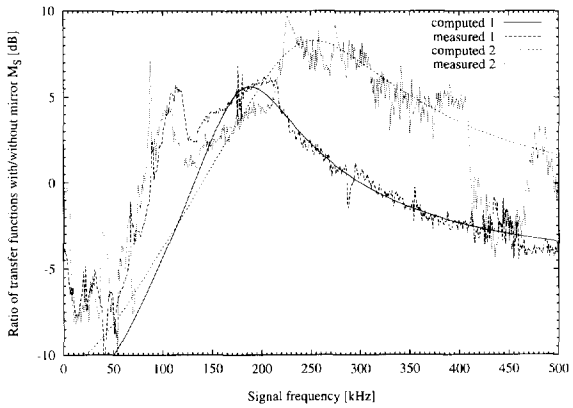

Fig. 6. Measured and computed ratio of transfer functions with and without signal extraction mirror M_S for the two schemes of controlling M_S.

by subtracting the instantaneous amplitude from U has the proper sign on both sides of the desired operating point. There are two degrees of freedom (U and $\Delta\phi$) which allow to select the desired tuning δ (and hence the detector's frequency response) in a wide range.

In order to measure the transfer function, test signals from 0–500 kHz (with amplitudes corresponding to mirror movements of less than 1 pm) were fed to M_{R2}. The magnitude of the output signal was simultaneously monitored at the signal frequency using a Marconi 2380/2382 spectrum analyzer, which was also used to generate the swept sine test signals. To observe the effect of the signal extraction mirror M_S, each measurement was repeated with M_S removed. The ratio of these two transfer functions was compared with the theoretically expected ratio

$$M(\omega,\delta) = \frac{H_1(\omega,\delta,\psi_{42}(\delta))}{H_1^0(\omega,\psi\equiv 0)}. \tag{8}$$

Here $H_1^0(\omega,\psi\equiv 0)$ is obtained from H_1 by setting $\rho_S = 0$, and $\psi_{42}(\delta)$ is described below.

In the interpretation of our data, special attention must be paid to the phase ψ of the Mach–Zehnder interferometer, since the interferometer's transfer function depends on ψ, as described in Section 2. Without M_S, the 42 kHz signal used to adjust ψ arrives at the output with a certain phase which we take as zero. The 42 kHz demodulator's reference phase was adjusted for this case and not changed afterwards. With M_S in place, however, the 42 kHz signal experiences a change in magnitude and phase according to Eq. (7). In our setup, the control loop for ψ continually maximizes the 42 kHz amplitude as determined by demodulation with the preset phase. This corresponds to maximizing $\mathrm{Re}[H_2(2\pi\times 42\ \mathrm{kHz},\delta,\psi)]$. We define the phase $\psi_{42}(\delta)$ by this maximum condition, in accordance with the ψ that appears in the experimental situation. It was computed numerically and was found to vary between -0.6 and $+0.6$ rad, depending on δ.

4. Results and conclusion

Fig. 6 shows the measured results. The ratios of the interferometer's measured transfer functions with and without mirror M_S are shown for the two different schemes of controlling M_S. The computed ratios are shown for comparison.

The curves labelled 1 refer to the first scheme (setting the peak sensitivity to 180 kHz by dithering M_S). The tuning δ was 0.584 rad (found by a nonlinear fit), and the corresponding Mach–Zehnder phase was

$\psi = \psi_{42}(\delta) = -0.336$ rad. At frequencies around and above the peak, theory and experiment agree reasonably well.

The discrepancies at lower frequencies were found to result from an interaction with the Pound–Drever systems used to keep the two arm cavities resonant. With M_S in place, the two cavities are no longer independent. The laser frequency is stabilized to the first cavity with a unity-gain frequency of approximately 120 kHz (without M_S). The gain of this loop is modified by M_S, because the detuned signal extraction cavity causes additional optical feedback and introduces extra phase shifts in the loop. This was verified by changing the overall loop gain of the frequency stabilization and observing a shift in frequency and height of the 120 kHz peak in Fig. 6.

Another effect is caused by the asymmetry between the two Pound–Drever systems. As described in Section 3, the second arm cavity is kept resonant with a unity-gain frequency of only a few 10 kHz, considerably lower than the 120 kHz of the first cavity loop. The test signal being fed into the second cavity appears, after reflection by M_S, as a frequency deviation on photodetectors PD1 and PD2. Here it is amplified and fed back to the laser frequency and the length of the second cavity, respectively. At those frequencies where some loop gain remains, the theory described in Section 2 is no longer valid, especially when the gains for the two arms are not identical.

Both these effects arise from our specific experimental setup and will not appear in the planned large-scale detectors if the laser frequency is stabilized to either an independent reference or to the power-recycling cavity instead of one arm cavity, and if the unity-gain frequency of the loops used to lock the arm cavities is below the observation bandwidth.

The curves labelled 2 were obtained by locking M_S with the second scheme (maintaining the 180 kHz output signal at a constant level). A sensitivity peak at approximately 250 kHz was obtained, corresponding to $\delta = 0.433$ rad. A constant of 1.8 dB had to be added to the theoretical curve for a best fit, which can be understood by the misalignment of the Mach–Zehnder interferometer introduced by removing M_S and the lens used to compensate the lensing effect of the curved mirror substrate. Around 420 kHz the PZT response was so small that both signals were buried in the noise. In further experiments (not shown), the sensitivity peak could be shifted to as high as 400 kHz, more than twice the calibration signal frequency.

5. Conclusion

We have, for the first time, operated a resonant sideband extraction interferometer at a detuned operating point. The frequency response agrees well with theory. A coupling of formerly independent loops by optical feedback was observed, and requires further investigation. Another interesting point is the detection of the signal sidebands by external modulation in a Mach–Zehnder type interferometer. We have confirmed experimentally the validity of the expressions describing the output in the general (detuned) case, Eqs. (3)–(7). In the detuned case of signal extraction or signal recycling, the phase of this Mach–Zehnder interferometer cannot be optimized for all signal frequencies simultaneously.

References

[1] A. Abramovici et al., Science 256 (1992) 325.
[2] C. Bradaschia et al., Nucl. Instr. Meth. Phys. Res. A 298 (1990) 518.
[3] K. Danzmann et al., in: Proc. first Edoardo Amaldi Conf. on Gravitational wave experiments, Frascati 1994 (World Scientific, Singapore, 1995).
[4] B.J. Meers, Phys. Rev. D 38 (1988) 2317.
[5] P.R. Saulson, Fundamentals of interferometric gravitational wave detectors (World Scientific, Singapore, 1994).
[6] J. Mizuno, Ph.D. Thesis, Universität Hannover and Max-Planck-Institut für Quantenoptik, Garching (1995); also available as MPQ-Report 203, July 1995.

[7] W. Winkler et al., Phys. Rev. A 44 (1991) 7022.
[8] W. Winkler et al., Opt. Commun. 112 (1994) 245.
[9] K.A. Strain et al., Phys. Lett. A 194 (1994) 124.
[10] J. Mizuno et al., Phys. Lett. A 175 (1993) 273.
[11] B.J. Meers, Phys. Lett. A 142 (1989) 465.
[12] J.A. Lobo, Class. Quantum Grav. 9 (1992) 1385.
[13] C.N. Man et al., Phys. Lett. A 148 (1990) 8.
[14] R.W.P. Drever et al., Appl. Phys. B 31 (1983) 97.
[15] K.A. Strain, private communication (1992).